

SNS 104050000-TD0010-R01

# Linac Halo Mitigation

January 2002



A U.S. Department of Energy Multilaboratory Project

SPALLATION NEUTRON SOURCE  
Argonne National Laboratory • Brookhaven National Laboratory • Thomas Jefferson National Accelerator Facility • Lawrence Berkeley National Laboratory • Los Alamos National Laboratory • Oak Ridge National Laboratory

This report was prepared as an account of work sponsored by an agency of the United States government. Neither the United States government nor any agency thereof, nor any of their employees, makes any warranty, express or implied, or assumes any legal liability or responsibility for the accuracy, completeness, or usefulness of any information, apparatus, product, or process disclosed, or represents that its use would not infringe privately owned rights. Reference herein to any specific commercial product, process, or service by trade name, trademark, manufacturer, or otherwise, does not necessarily constitute or imply its endorsement, recommendation, or favoring by the United States government or any agency thereof. The views and opinions of authors expressed herein do not necessarily state or reflect those of the United States government or any agency thereof.

# LINAC HALO MITIGATION

SNS/AP TECHNICAL NOTE

D. Jeon, J. Stovall, A. Aleksandrov, J. Wei, ORNL  
J. Staples, R. Keller, LBNL  
L. Young, H. Takeda, LANL

January 15, 2002

Prepared for the  
U.S. Department of Energy  
Office of Science

UT-BATTELLE, LLC  
managing  
Spallation Neutron Source activities at  
Argonne National Laboratory      Brookhaven National Laboratory  
Thomas Jefferson National Accelerator Facility      Lawrence Berkeley National Laboratory  
Los Alamos National Laboratory      Oak Ridge National Laboratory  
under contract DE-AC05-00OR22725  
for the  
U.S. DEPARTMENT OF ENERGY



# CONTENTS

	<b>Page</b>
LIST OF FIGURES.....	v
1. SUMMARY .....	1
2. INTRODUCTION.....	1
3. DTL COLLIMATION .....	5
4. PROPOSED PLANS.....	10
4.1 MEBT SCRAPING .....	10
4.2 ALTERNATIVE MEBT OPTICS.....	13
4.3 HYBRID HALO SOLUTION.....	15
5. LEBT SCRAPING.....	16
6. CONCLUSION.....	18
ACKNOWLEDGEMENT .....	18
REFERENCE.....	18
APPENDIX 1 .....	A-1
APPENDIX 2 .....	A-2
APPENDIX 3 .....	A-3



## LIST OF FIGURES

Figure	Page
2.1	Phase-space projections of the measured and simulated LEBT beam ..... 2
2.2	Transverse ( $x-x'$ and $y-y'$ ) phase-space projections of the beam distribution at the RFQ exit. .... 2
2.3	Transverse ( $x-x'$ and $y-y'$ ) phase-space projections of the measured beam distribution at the DTL entrance showing horizontal tails which have developed in the chopper..... 3
2.4	Transverse beam envelope profiles in the MEBT ..... 3
2.5	Radial particle distribution of the “measured” beam at 171 MeV assuming no linac errors showing a significant halo extending beyond the CCL bore..... 4
3.1	Schematic diagram of DTL tank 1 showing the location of proposed collimators ..... 5
3.2	Real space projections of the beam distribution at the MEBT chopper target and at the first 7 of the proposed DT collimators. .... 6
3.3	Expected energy deposited in 8mm radius DTL apertures ..... 7
3.4	Radial beam distribution at 171MeV with and without DTL collimation ..... 8
3.5	Radial beam distribution at 171MeV with and without DTL collimation ..... 8
3.6	Expected energy deposited in 6 mm radius DTL apertures ..... 9
3.7	Real-space beam distribution at the end of DTL tank 1 for one set of random machine imperfections ..... 9
4.1.1	Schematic layout of the MEBT indicating the location of adjustable horizontal scrapers at the chopper target (red arrow)..... 11
4.1.2	Schematic drawing of adjustable MEBT scrapers and chopper target..... 11
4.1.3	Beam profile at 171MeV with (red curve) and without MEBT collimation (blue curve) at $\pm 8$ mm ..... 12
4.1.4	Maximum and minimum power corresponding to beam particles outside a radius of 8 mm in empty drift tubes after passing through a $\pm 8$ -mm MEBT scraper ..... 12

4.2.1	Beam envelope profiles of the modified MEBT optics yielding a more circular cross section in the anti-chopper .....	13
4.2.2	Radial beam distribution at 171MeV corresponding to a modified MEBT optics design (red) showing 87% reduction in beam halo .....	14
4.2.3	Beam projections at the ring injection foil of a partially chopped but unrestored beam (blue) using alternate MEBT optics compared with the nominal unchopped design (red).....	15
4.3.1	Radial beam distribution at 171MeV for the hybrid halo mitigation solution .....	16
5.1	Phase-space projections of the measured and simulated LEBT beam in which the LEBT is terminated in a 4 mm aperture .....	17
A.1	Trace3D output of entire MEBT optics modification .....	A-1
A.2	Beam profile plots at 171MeV for three different MEBT optics without any collimation.....	A-1
A.3	Schematic drawing of beam scraper for the Drift-Tube-Linac of the 200 MeV Linac at Brookhaven National Laboratory.....	A-2

## 1. ABSTRACT

The SNS beam distribution, based on Front End (FE) emittance measurements and multiparticle simulation studies, develops a substantial halo that leads to beam loss and radio activation of the SNS linac. The DOE has recommended that we “develop a plan that would permit insertion of collimators in DTL tank #1” to remove the halo.

This recommendation has been evaluated and we find that this approach does not substantially reduce the halo, but would impose infeasible thermal loads on the drift tubes. Three additional techniques have been studied, involving LEBT and MEBT collimation and modified MEBT optics. Based on the results of these studies it appears that we have identified an alternate scenario that looks highly promising for reducing beam halo.

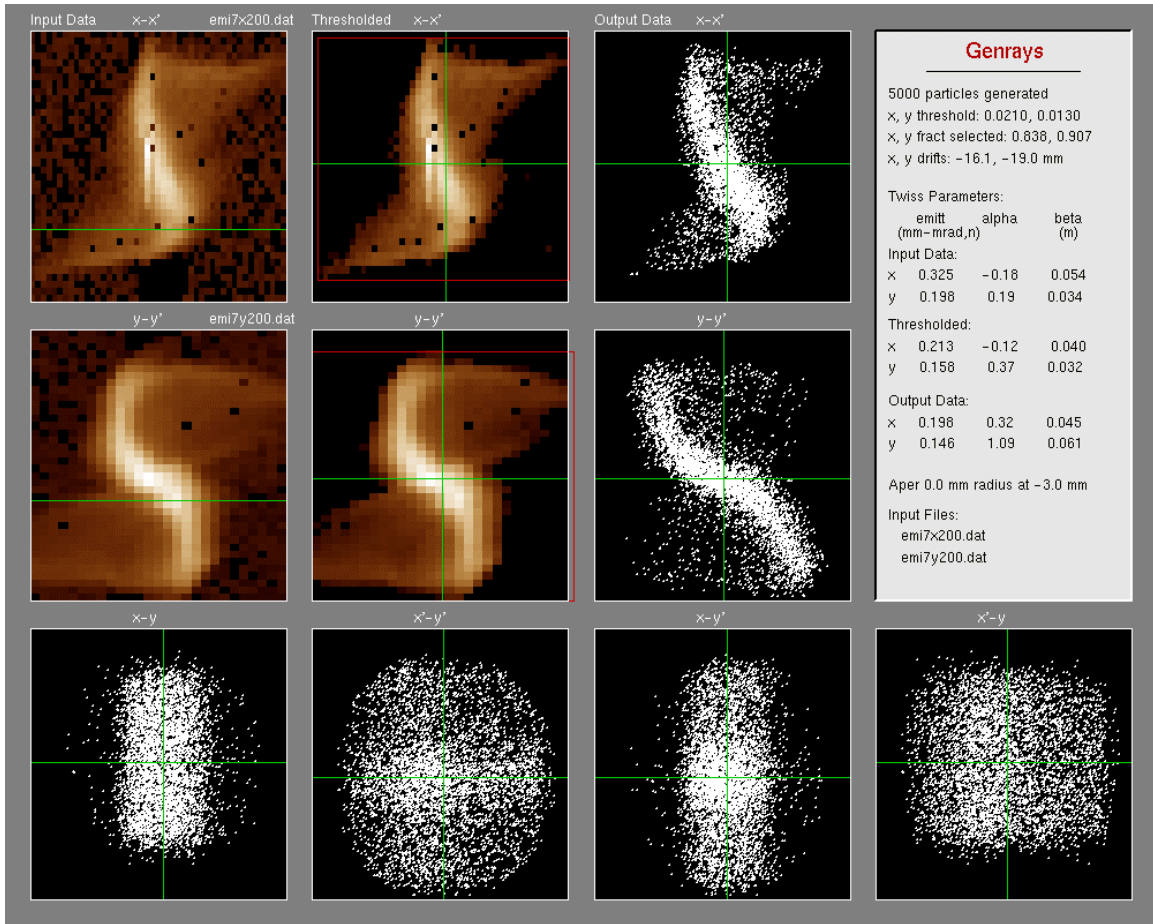
## 2. INTRODUCTION

The Spallation Neutron Source accelerator system is designed to accelerate intense proton beams to an energy of 1-GeV, delivering more than 1 MW of beam power to the neutron production target. A primary concern is potential damage and radio activation of accelerator components resulting from uncontrolled beam losses. A major source of loss is beam halo that intercepts the bore of the linac. Presently, beam halo scrapers and collimators are implemented only in the High-Energy Beam-Transport (HEBT) line, the accumulator ring, and the Ring-Target Beam-Transport (RTBT) line. These scrapers do not protect the linac because they follow the linac exit.

Beam dynamics simulations show that the beam halo develops at low energy, but some halo particles survive acceleration to higher energies before being lost on the linac bore. This particle loss at higher energies results in radio activation of the Coupled-Cavity Linac (CCL). Whatever halo survives the linac may likewise escape HEBT collimation and increase the heat load in the ring-injection beam dump.

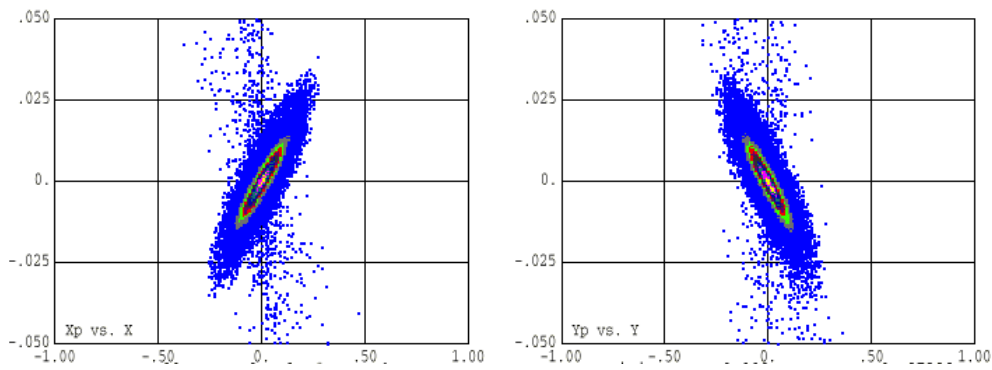
Several FE components and physical effects may contribute to the generation of beam halo. These include details of the ion-source design, plasma dynamics and extraction optics, nonlinear LEBT optics, phase-space mismatch between the LEBT and the radio frequency quadrupole (RFQ) linac, the RFQ itself, and the MEBT. The MEBT is the largest contributor to beam halo. The beam phase width is large enough so that nonlinear fields in the buncher gaps cause halo growth. More importantly, because the beam has a large transverse eccentricity over a relatively long distance, it experiences nonlinear space-charge forces and develops “tails” in the transverse phase-plane projections. In the Drift-Tube Linac (DTL), these tails develop into a halo that is inseparable from the core of the beam.

Figure 2.1 shows the measured beam emittance in the LEBT upon which we based our beam-dynamics simulations. The upper row of plots shows  $x-x'$  projections and the second row shows  $y-y'$ . The two colored plots in the first column show the raw emittance data. The second column shows the “analyzed” data after applying a threshold to eliminate noise and spurious signals. The third column shows the macroparticle distribution that we derived from the analyzed data and that we used in our numerical simulations. The derivation algorithm assumed a particular type of distribution for the unmeasured correlations in the real beam distribution. The bottom row shows these four projections generated for the numerical distribution:  $x-y$ ,  $x'-y'$ ,  $x-y'$  and  $x'-y$ .



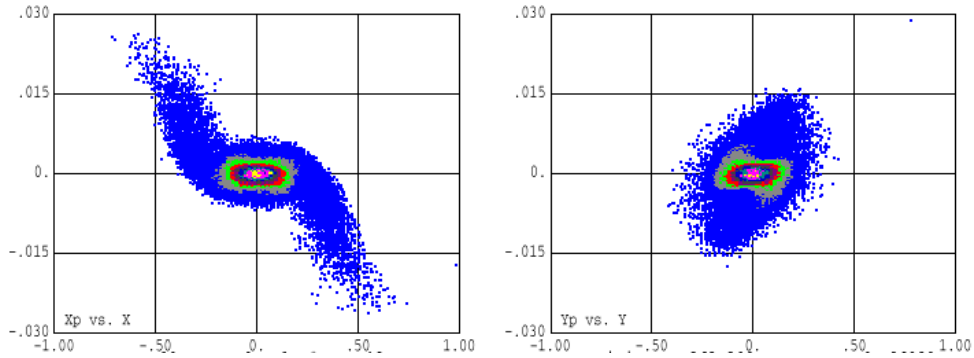
**Fig. 2.1. Phase-space projections of the measured and simulated LEBT beam.**

Figure 2.2 shows the transverse phase-space projections of the measured beam transported to the RFQ exit. The particles that appear to be scattered in the angular dimension correspond to low energy particles ( $\sim 0.1\text{MeV}$ ) that are destined to be lost longitudinally at low energies and are of no concern. Otherwise, this beam is only slightly worse than one originating from an initial water-bag distribution at the RFQ entrance.



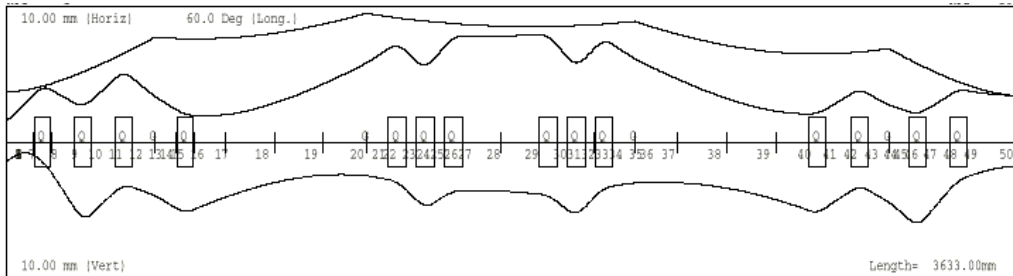
**Fig. 2.2. Transverse ( $x-x'$  and  $y-y'$ ) phase-space projections of the beam distribution at the RFQ exit.**

Figure 2.3 shows the transverse phase-space projections of the beam at the entrance to the DTL. The now well-developed tails in the horizontal projection are a result of the MEBT optics, which maintains the beam eccentricity of  $\sim 2:1$  throughout the  $\sim 1.6$ -m-long chopper section.



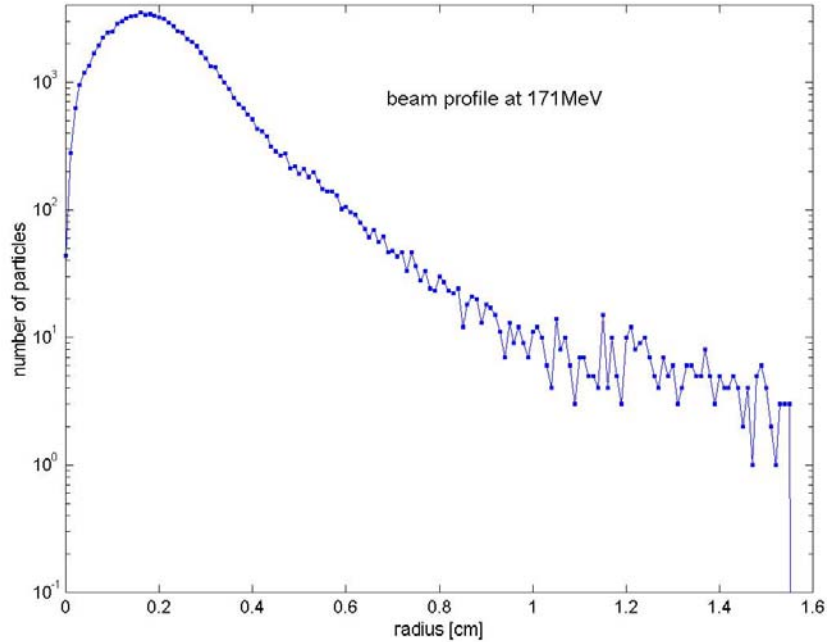
**Fig. 2.3. Transverse ( $x-x'$  and  $y-y'$ ) phase-space projections of the measured beam distribution at the DTL entrance showing horizontal tails which have developed in the chopper.**

Figure 2.4 shows the horizontal (upper) and vertical (lower) envelope profiles of the beam in the MEBT. The beam is squeezed vertically to clear the vertical deflection plates of both the chopper and anti-chopper.



**Fig. 2.4. Transverse beam envelope profiles in the MEBT.**

In the DTL, the energy associated with the horizontal tails quickly gets redistributed, resulting in a halo in both horizontal and vertical emittance projections. We are, of course, concerned with any increase in the effective emittance of the beam, but more importantly in any increase in the real-spatial size of the beam, which increases the risk of interception with the linac bore. The radial particle distribution in Fig. 2.5 shows that even without including any errors in the beam dynamics simulation, at the end of the CCL the halo extends beyond the 1.5-cm physical bore radius. Throughout the CCL the focusing strength of the transverse lattice gradually weakens to smoothly match the focusing strength in the Superconducting (SRF) linac. As a result, the beam size is largest near the end of the CCL, so that most of the beam loss occurs at energies near 170 MeV. By including random errors in the simulations we readily see the locations of “hot spots” caused by beam loss.



**Fig. 2.5. Radial particle distribution of the “measured” beam at 171 MeV assuming no linac errors showing a significant halo extending beyond the CCL bore.**

Our simulations indicate that, without cleaning, the beam halo results in excessive beam loss in DTL and CCL. Furthermore, the halo effectively increases beam emittance and causes more particles to miss the injection foil. We have investigated the effectiveness and feasibility of four schemes for reducing the halo, including drift-tube collimation suggested by the DOE. We propose an alternate, more flexible scheme that can be progressively implemented, as necessary. The proposed scheme has little or no impact on the construction schedule. Given the uncertainty of the beam distribution from the LEBT, our goal is to implement a robust system that can accommodate varying commissioning and operating beam conditions.

### 3. DTL COLLIMATION

The DOE has directed us to develop a plan that would permit the insertion of scrapers into drift tubes in tank 1 that would trim off the beam halo described above. The focusing lattice in the DTL is FFODDO, where O means empty drift tubes. We considered inserting circular collimators in the first 11 empty drift tubes. By using only empty drift tubes, we avoid the possibility of overheating and possibly approaching the Curie point of the permanent-magnet quadrupole lenses (PMQs). In addition, the beam is nearly round in the empty drift tubes making collimation by circular apertures more effective.

The first 5 lattice periods, spanning 30 drift-tubes, represents a depressed phase advance of about  $2\pi$  radians. Therefore, by placing collimators in the first 10 or 11 empty drift tubes should trim off the halo, assuming that the halo remains on the perimeter of the beam. The aperture size would have to follow the beam size. Figure 3.1 shows schematically the first half of DTL tank 1. The colored drift tubes contain PMQs. The vertical red arrows show the proposed locations of collimators.

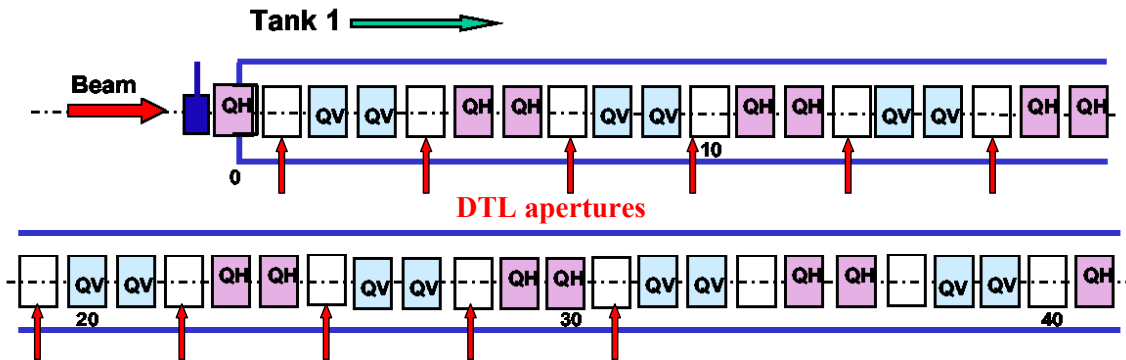
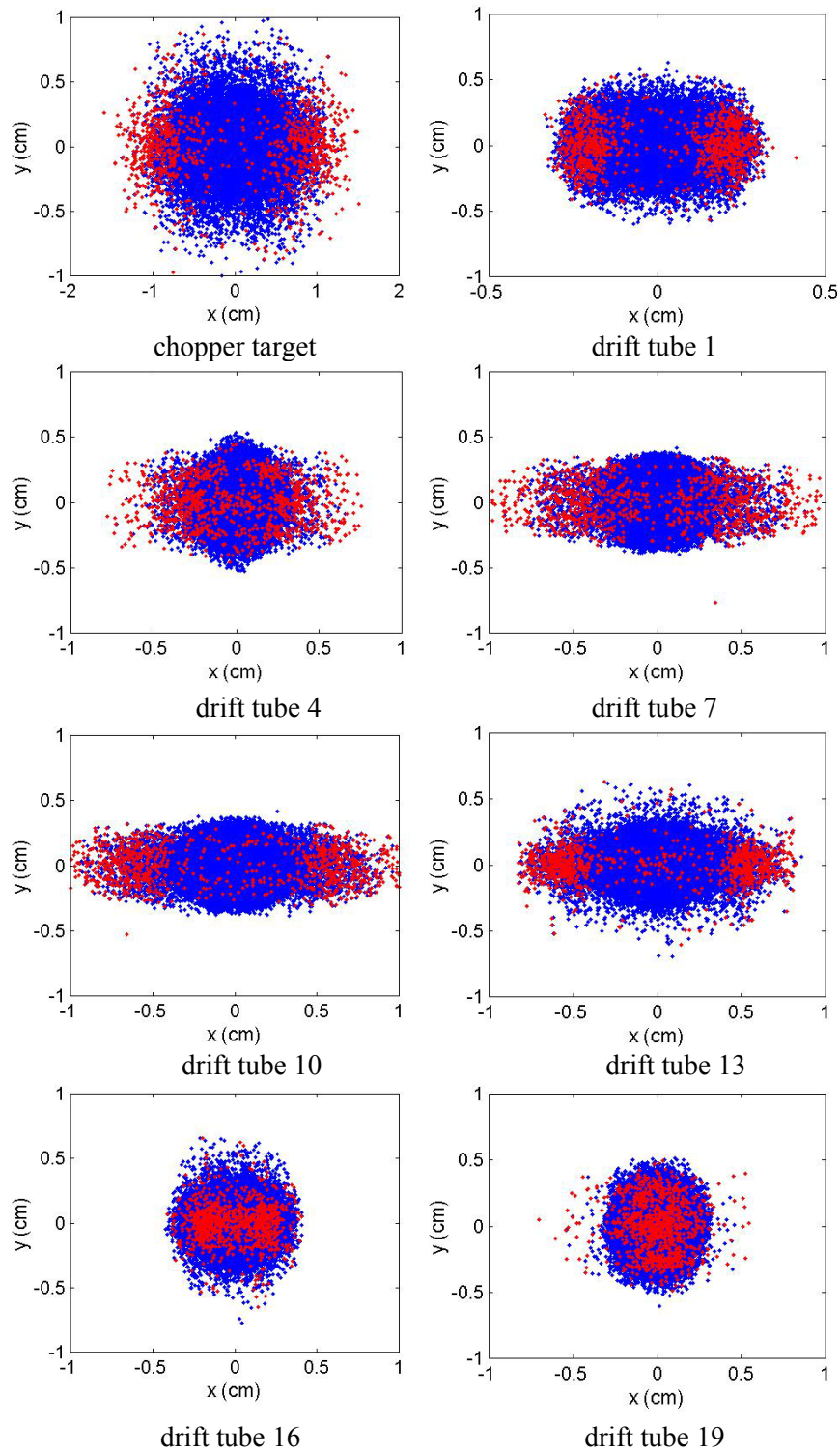


Fig. 3.1. Schematic diagram of DTL tank 1 showing the location of proposed collimators.

We predict the effectiveness of the collimation scheme by identifying the halo particles “at risk” as the outermost 1%, which corresponds to those having a radius greater than 0.9 cm in Fig. 2.5. We then track these particles through the DTL. Figure 3.2 shows the real-space projections of the beam at the chopper target and at the first 7 locations of the drift-tube collimators. The “at risk” particles are plotted in red.



**Fig. 3.2. Real space projections of the beam distribution at the MEBT chopper target and at the first 7 of the proposed DT collimators. Halo particles “at risk” are plotted in red.**

Halo particles have more transverse energy than do core particles. They oscillate through the core with large amplitudes, spending only part of their time on or near the beam perimeter. The projections in Fig. 3.2 clearly show halo particles inside the core of the beam. In fact, the halo is completely unobserved at some points (e.g. drift tubes 1 and 16). The tails created in the MEBT have become so well integrated with the core of the beam that drift-tube collimation is not effective.

To evaluate the effectiveness of DTL collimators, we looked at the radial particle distribution at 171 MeV for several collimator radii. To evaluate their feasibility, we calculated the amount of energy deposited in each drift tube from scraped beam. This energy represents an addition to the rf thermal load on each drift tube. The water-cooling circuit must remove this heat in order to hold the structure on resonance.

We first considered 8-mm-radius circular collimators and transported the beam without including errors such as misaligned drift tubes. The collimators reduce the bore cross section by 36%, but trim just 0.22% from the beam. The left-hand plot of Fig. 3.3 is the expected power deposited in the collimating drift tubes. The maximum power of  $\sim 5$  W deposited in drift tube 10 adds 10% to the rf heat load. The expected beam-loss profile compared with the beam sizes in Fig. 3.2 shows that the beam completely clears the apertures in drift tubes 13, 16 and 19, so there is no beam power added to these drift tubes.

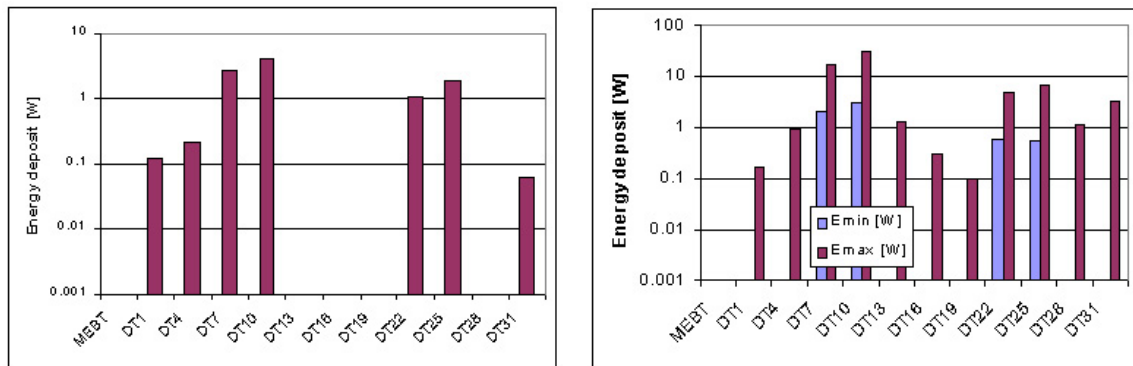


**Fig. 3.3. Expected power deposited in 8mm radius DTL apertures.** The right-hand plot assumes no errors. The left-hand plot summarizes the results of 100 linac runs with errors.

The first dipole corrector in DTL tank 1 is in drift tube 49, so there is no steering spanning the proposed collimators. With this lack of steering, it is prudent to study the effects of machine imperfections. The right-hand plot of Fig. 3.3 summarizes the simulated particle dynamics in 100 linacs that included random alignment errors. The plot shows the maximum and minimum power lost at each aperture. The maximum power, again at drift tube 10, was 31W, adding 65% to rf heating.

The radial particle distributions plotted in Fig. 3.4 show the effectiveness in reducing halo by 8-mm drift tube collimators. The blue curve is the radial beam distribution at 171 MeV without collimation, and the red curve is the distribution after being trimmed. Even though 0.22% of the beam has been trimmed from the beam there is no observable reduction in the beam halo.

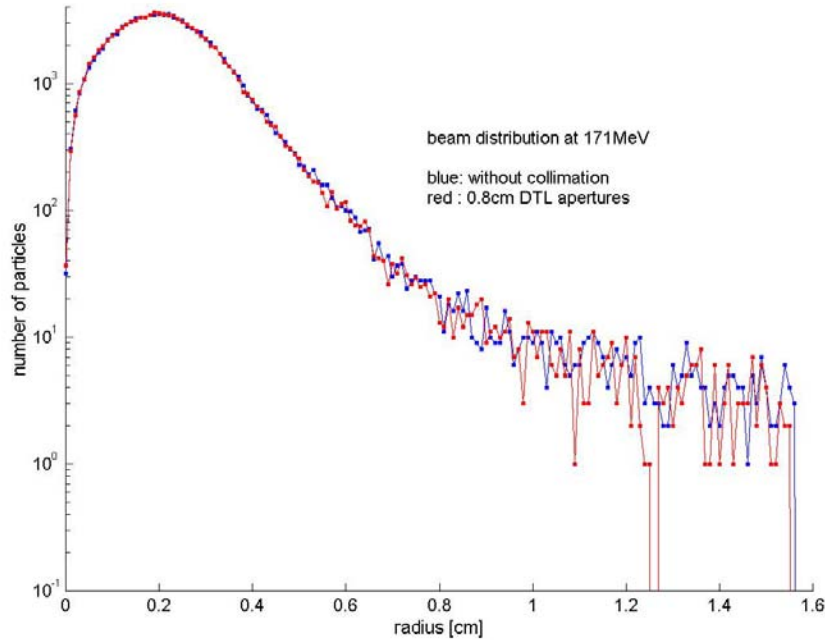


**Fig. 3.4. Radial beam distribution at 171 MeV with and without DTL collimation.** DTL apertures of 8-mm radius do not reduce beam halo.

Next we considered 6-mm-radius collimators, which reduces the bore cross section by 64%. Indeed, the beam halo at 171 MeV is reduced as shown in Fig. 3.5. The smaller apertures remove over 1% of the beam and reduce the current in the halo ( $r > 1.1$  cm) by 90%. Unfortunately, the energy deposited in the 6-mm apertures is excessive.

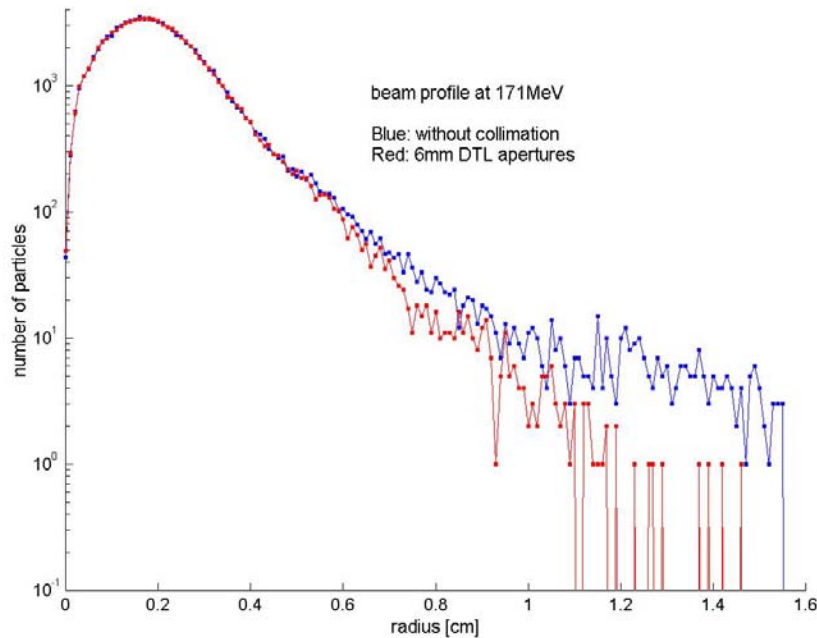


**Fig. 3.5. Radial beam distribution at 171 MeV with and without DTL collimation.** Apertures of 6-mm radius reduce beam halo by 90%, but result in excessive drift tube heating.

The left-hand plot of Fig. 3.6 shows that, excluding errors, the beam power deposited in drift tube 10 would double the design thermal load. Including errors (right-hand plot of Fig. 3.6), the maximum expected power deposited in drift tube 22 is 444 W, which is ~6 times the design cooling capacity of this drift tube.

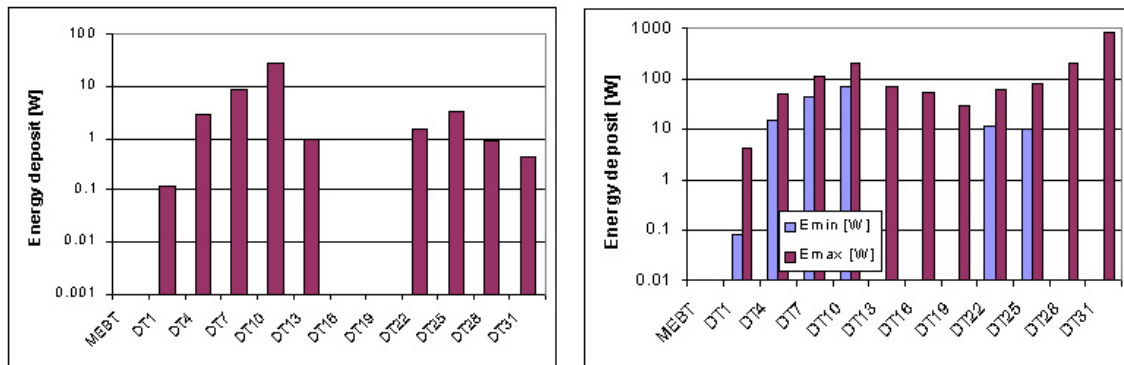


**Fig. 3.6. Expected energy deposited in 6 mm radius DTL apertures.** The left-hand plot assumes no errors. The right-hand plot summarizes the results of 100 linac runs with errors.

The random misalignment of the PMQs steers the beam, so the beam centroid is seldom on axis. Without beam-position monitors (BPMs) in the low-energy end of tank 1 we have no way to steer the MEBT beam onto the DTL axis. As a consequence, the beam will scrape the bore asymmetrically as shown in Fig. 3.7. Although we did not quantify this effect, it is clear that even small drift-tube apertures would not assure a significant reduction in the halo, but would guarantee serious heating problems.

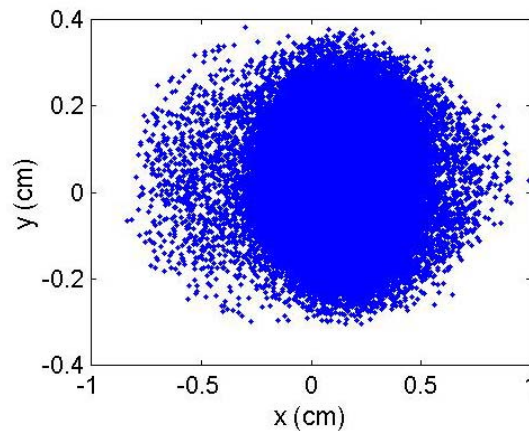


**Fig. 3.7. Real-space beam distribution at the end of DTL tank 1 for one set of random machine imperfections.** The resulting asymmetric scraping leaves a significant halo.

We conclude that placing apertures in drift tubes is neither an effective nor safe approach to removing halo particles that are expected to be lost in an uncontrolled way.

- Too small an aperture (~6-mm radius) is required to effect any useful reduction in the beam halo.
- Severe thermal loading of the drift tubes will exceed the ability of the present drift-tube cooling design.
- Apertures of fixed size and shape lack the flexibility required to accommodate beam matching and steering.
- Asymmetric scraping is expected to result from unpredictable construction and steering errors that would nullify any expected benefit.

## 4. PROPOSED PLANS

We propose an alternate scheme for halo mitigation that reduces the opportunity for formation of transverse tails, and trims the tails before they have an opportunity to mix with the beam core. The proposed scheme utilizes adjustable scrapers at the location of the MEBT chopper target and/or adjustable scrapers in the anti-chopper box (in the case that anti-chopper is unnecessary). We also need three more power supplies to make the MEBT quadrupoles independently adjustable, thus providing adjustable MEBT optics to control beam halo generation.

### 4.1 MEBT SCRAPING

There are only a few places where scrapers will fit in the MEBT. One convenient place is at the chopper target. Figure 4.1.1 shows the layout of the MEBT. A pair of adjustable horizontal scrapers would be installed in the chopper target box (at the red arrow). The chopper target itself is located above the mid-plane to intercept beam that is deflected upward. Scrapers mounted on horizontal actuators will not interfere with the function of the target. This assembly is shown schematically in Fig. 4.1.2. This scraper implementation has the advantage that it is readily adjustable to accommodate the actual beam conditions, which are expected to vary with different operating conditions such as beam current, ion-source performance, LEPT, RFQ, and MEBT tuning.

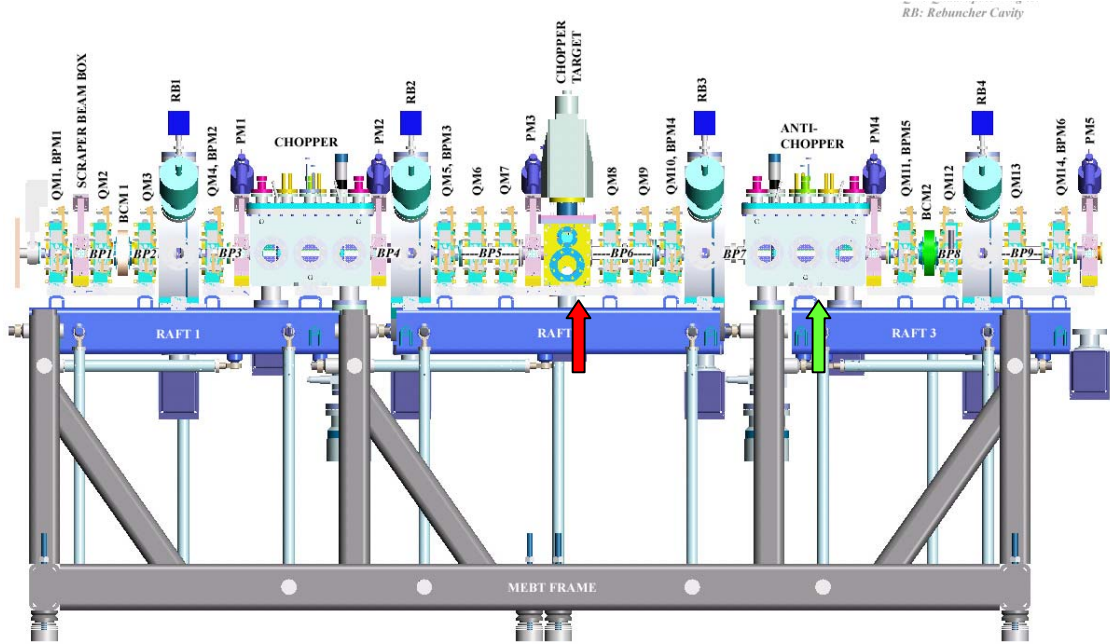


**Fig. 4.1.1. Schematic layout of the MEBT indicating the location of adjustable horizontal scrapers at the chopper target (red arrow). A second 4-jaw adjustable aperture could replace the anti-chopper as a backup (green arrow).**

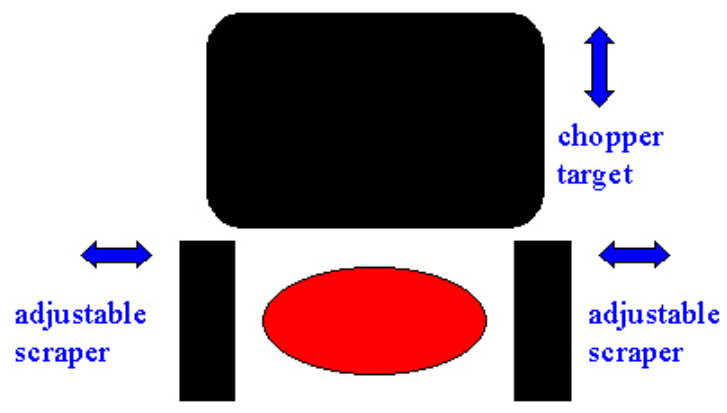


**Fig. 4.1.2. Schematic drawing of adjustable MEBT scrapers and chopper target.**

To compare with the DTL aperture study, we fixed the horizontal MEBT scraper aperture at  $\pm 8$  mm (see Fig. 3.2). Figure 4.1.3 shows that, without errors, the halo is reduced by 84%. We then ran 100 beam-dynamics simulations through the DTL including errors. To compare MEBT scraping with DTL scraping, we counted (and summed the energy of) halo particles whose radius exceeded 8 mm at empty drift tubes in tank 1. As indicated in Fig. 4.1.4, only a small fraction of beam particles experienced radial excursions greater than 8 mm. In the worst case, the corresponding power amounts to less than 5 W. For a comparable reduction in halo, DTL scraping causes 90 times this power loss. These results suggest that MEBT collimation may be sufficient.

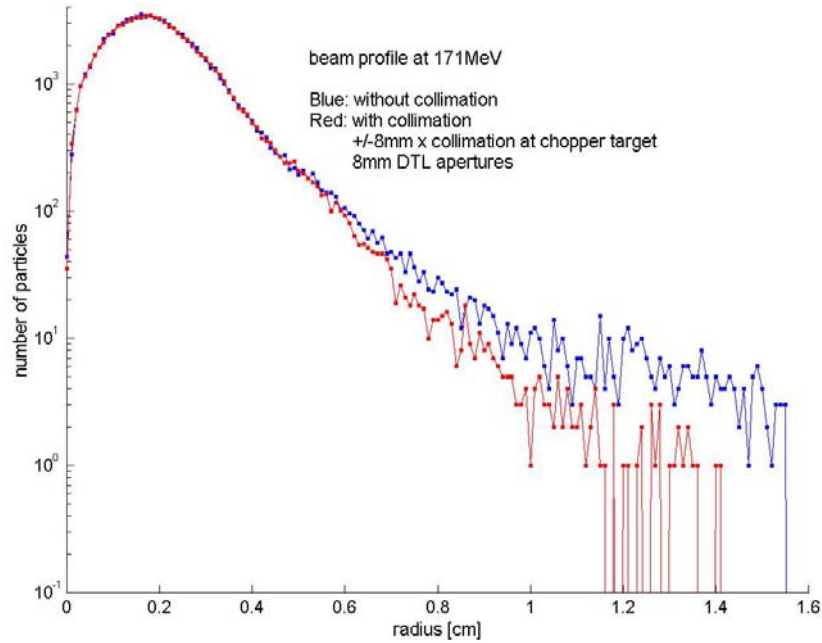


**Fig. 4.1.3. Beam profile at 171MeV with (red curve) and without MEBT collimation (blue curve) at  $\pm 8$ mm. Halo is reduced by 84%.**

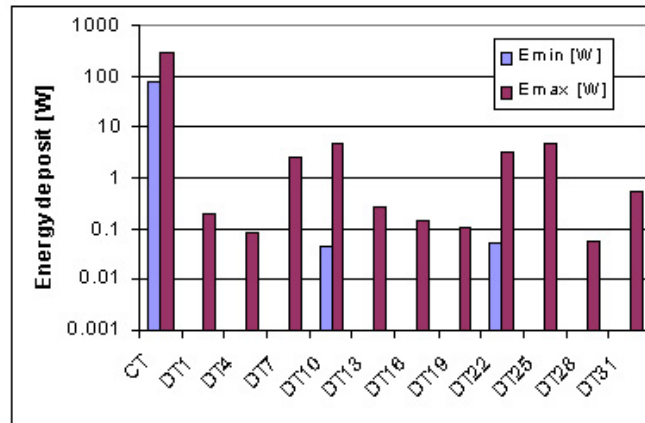


**Fig. 4.1.4. Maximum and minimum power corresponding to beam particles outside a radius of 8 mm in empty drift tubes after passing through a  $\pm 8$ -mm MEBT scraper. Column “CT” corresponds to beam scraped in the MEBT.**

## 4.2 ALTERNATIVE MEBT OPTICS

We believe that the primary cause of halo generation is nonlinear space-charge forces acting on a beam having a large transverse eccentricity. This condition occurs in both the MEBT chopper and anti-chopper where the beam is compressed vertically to facilitate chopping. The MEBT anti-chopper ideally operates at a vertical betatron phase of 90 degrees (zero-current phase advances) from the chopper target, and 180 degrees from the MEBT chopper, to restore any unchopped portion of the beam to its “original” position in phase space. Figure 2.4 shows that this condition produces a beam profile that is symmetric about the chopper target.

In an alternative design, we preserve the 90° phase advance from the chopper to the target, but we relax it to 63° from the target to the anti-chopper. The resulting beam cross section is more circular as shown in Fig. 4.2.1. Now, the anti-chopper no longer restores a partially chopped portion of the beam to its original (on-axis) position in phase space, if indeed that were desirable. Also, the beam now has a larger vertical extent and approaches the anti-chopper plates as designed. Alternative modes of anti-chopper operation are under study.

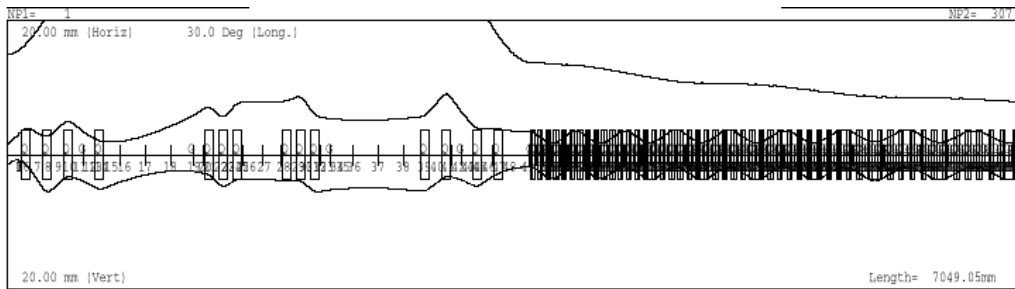


**Fig. 4.2.1. Beam envelope profiles of the modified MEBT optics yielding a more circular cross section in the anti-chopper.**

This simple modification to the optics reduces the formation of transverse tails and improves the beam quality in the downstream linac. Figure 4.2.2 shows that beam halo at 171MeV is reduced by 87%. The only expense of this marked improvement is providing independent adjustment of the two MEBT quadrupole triplets. The halo reduction is comparable to the effect of MEBT collimation for the baseline MEBT optics, but involves no beam loss at all.

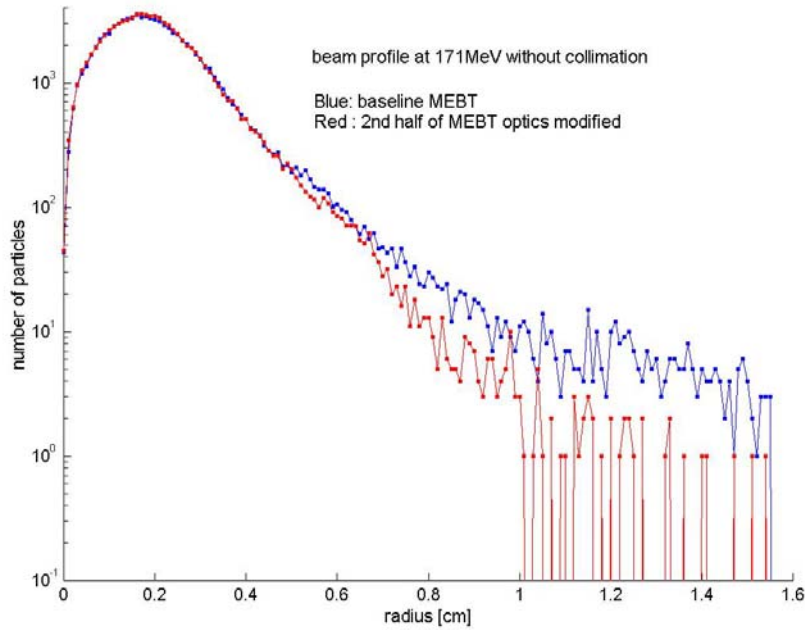


**Fig. 4.2.2. Radial beam distribution at 171MeV corresponding to a modified MEBT optics design (red) showing 87% reduction in beam halo.** The blue line corresponds to the baseline.

To realize this alternative optics scenario, three additional power supplies are needed to provide independent tuning of the quadrupole triplets. While the anti-chopper will not completely restore a partially chopped beam, it may not be required. Figure 4.2.3 shows that even without the anti-chopper, a partially chopped beam remains inside the envelope of the nominal beam at the foil. In this simulation, the chopper deflected the beam so that 50% of it was removed at the chopper target. This result is consistent with an earlier study by B. Blind (LANL), and strongly suggests that we adopt the proposed alternative MEBT optics with or without the anti-chopper.

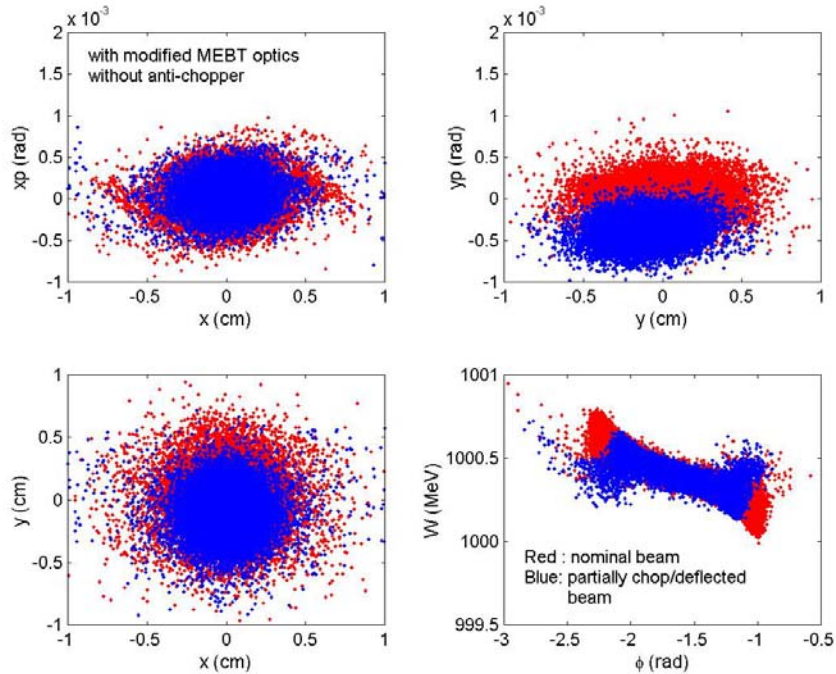


**Fig. 4.2.3. Beam projections at the ring injection foil of a partially chopped, but unrestored, beam (blue) using alternate MEBT optics compared with the nominal unchopped design (red). The partially chopped and deflected beam remains within the envelope of the nominal beam.**

### 4.3 HYBRID HALO SOLUTION

We also investigated the effectiveness of adding MEBT collimation in combination with the alternative optics design. In this scenario, we added MEBT collimation at the two locations indicated by arrows in Fig. 4.1.1. We adjusted horizontal scrapers to  $\pm 8$  mm at the chopper target and introduced a square aperture of  $\pm 6$  mm in the anti-chopper box. Figure 4.3.1 shows the radial beam distribution at 171 MeV resulting from this hybrid solution. The halo is reduced to only 3% of the baseline case.

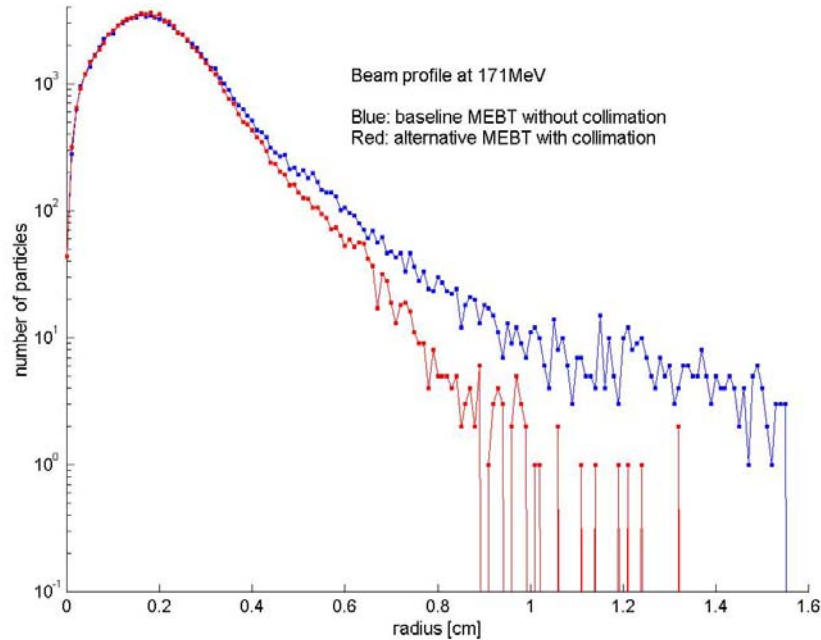


**Fig. 4.3.1. Radial beam distribution at 171MeV for the hybrid halo mitigation solution.** The red curve shows a 97% reduction in the halo with the combination of two collimators and modified MEBT optics. The blue line corresponds to the baseline performance.

Modifying the MEBT to create a more circular beam profile clearly eliminates much of the halo seen in the baseline design. In addition, with the introduction of variable collimators, we expect to reduce uncontrolled beam loss associated with halo to a manageable level.

- The alternative MEBT optics reduces beam halo formation.
- Additional beam scraping in the MEBT removes potential halo created in the chopper before it becomes integrated into the core.
- Implementation of the hybrid solution costs little and has no impact on schedule.
- Because the quadrupole lenses and all the scrapers are adjustable, this scheme works in any operational scenario.
- By tailoring the beam in the MEBT, rather than in the linac, its final quality will be insensitive to construction errors.
- MEBT scrapers intercepting  $\leq 1\%$  of the beam can be cooled.

## 5. LEBT SCRAPING

The beam produced by the ion source and subsequently accelerated through the LEBT exhibits a distorted projection in phase space (see Fig. 2.1). A poor shape of the H-minus emitting meniscus is primarily responsible for the distortion. The present design of the outlet aperture and extraction electrode produces a meniscus that emits a more divergent beam than desired. The beam further encounters increased spherical aberration in the LEBT elements, as it does not match the beam size assumed for the LEBT design.

At the exit of the LEBT, in the second of two einzel lenses, the LEBT chopper deflects the beam into a grounded target at the end of the LEBT, which also serves as a diagnostic element. This aperture currently has a diameter of 7.6 mm. Reducing the aperture diameter of this diagnostic element would remove some of the peripheral beam, which will reduce slightly the halo present in the RFQ beam. This change increases the on-off ratio of the LEBT chopper, and it reduces slightly the spherical aberration of the last lens. LEBT transmission will be slightly reduced.

We performed a beam-dynamics simulation with the exit aperture reduced from 7.6 mm to 4.0 mm. The input beam is modeled on experimental data taken 22 October 2001 with the potential of both einzel lenses set at -40 kV, the settings that result in maximum simulated beam through the RFQ. Figure 2.1 shows the generation of an input ensemble with the 7.6-mm aperture diameter at the LEBT exit. Figure 5.1 shows the generation of an input ensemble with a 4.0-mm aperture diameter at the LEBT exit. Reducing the aperture reduced transmission to the exit of the LEBT in the simulation by 3.8%.

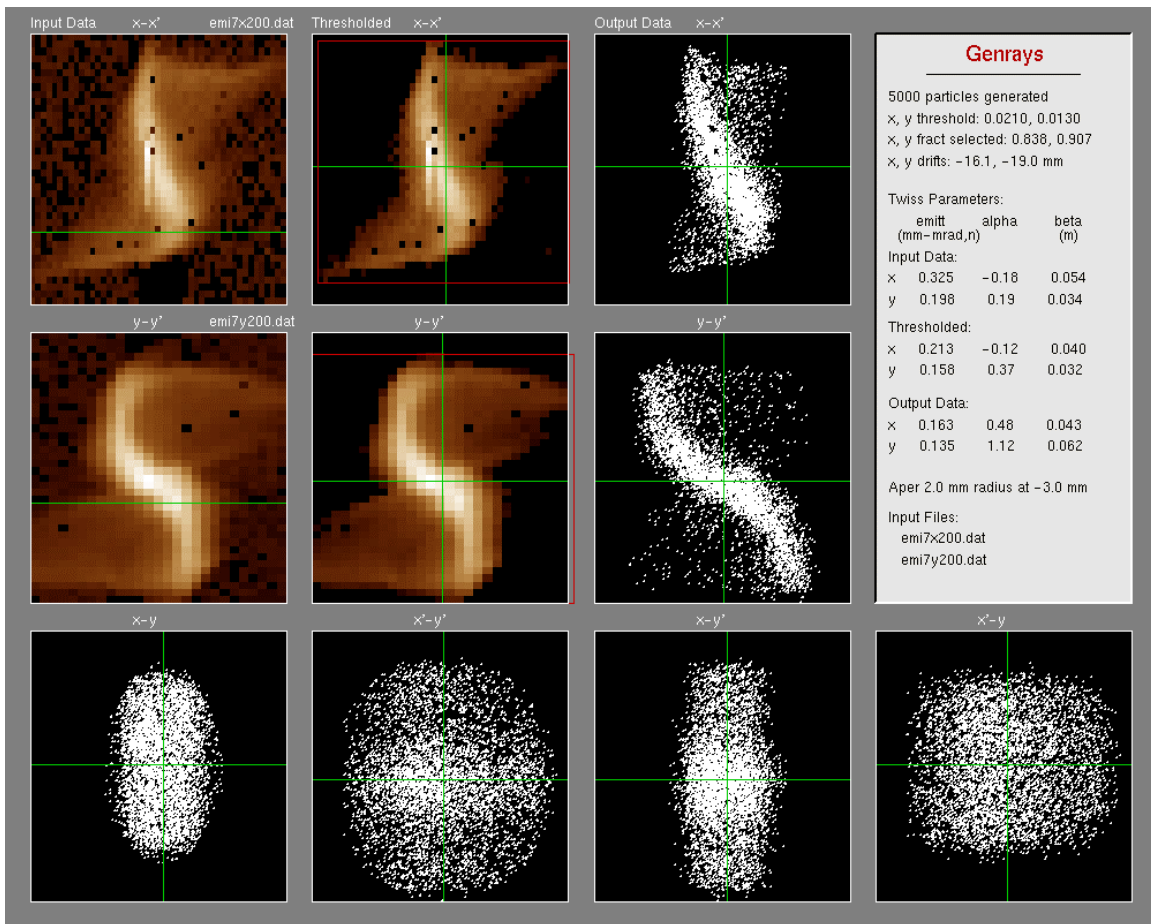


**Fig. 5.1. Phase-space projections of the measured and simulated LEBT beam in which the LEBT is terminated in a 4 mm aperture.**

We used the code Toutatis to transport both particle ensembles through the RFQ with a 38-mA current. The beam from the RFQ was then transported through the MEBT, using the latest tune derived by LANL and then through the room-temperature linac to an energy of 187 MeV using the Parmila code. Differences observed in the halo from these two distributions are statistically insignificant.

## 6. CONCLUSION

After investigating the potential for mitigating halo by introducing apertures in the DTL, we conclude that this scheme is neither effective nor practical. Too small an aperture is required to reduce halo significantly, and results in severe thermal loading of the drift tubes. Asymmetric scraping, resulting from errors would nullify any potential benefit. Fixed apertures would limit our ability accommodate any variety of beam conditions.

Modifying the MEBT optics and introducing adjustable scrapers as needed is a preferred alternative for mitigating halo by preempting its formation. The hybrid solution does not involve any redesign that would impact the construction schedule. Because the lenses and scrapers are all adjustable, this scheme is adaptable to any operational scenario.

## ACKNOWLEDGEMENT

We would like to thank G. Murdoch, D. Raparia, et al for having provided information on the beam scraping at ISIS and BNL.

## REFERENCES

- [1] Jim Stovall *et al*, “Final design & expected beam performance of SNS linac”, ASAC Review, September 2001.

## APPENDICES

### Appendix 1: Halo enhancement in MEBT

Beam halo can be significantly reduced with revised MEBT optics. In the unlikely case that MEBT chopper can be avoided, one can further relax the beta function at the MEBT chopper using the independent MEBT triplet quadrupoles. Entire MEBT optics is modified, unlike the MEBT optics modification mentioned in the Proposed Plan section. The Trace3D output is shown in Fig. A.1. Figure A.2 compares the amount of beam halo at 171MeV for the same input beam into the MEBT.

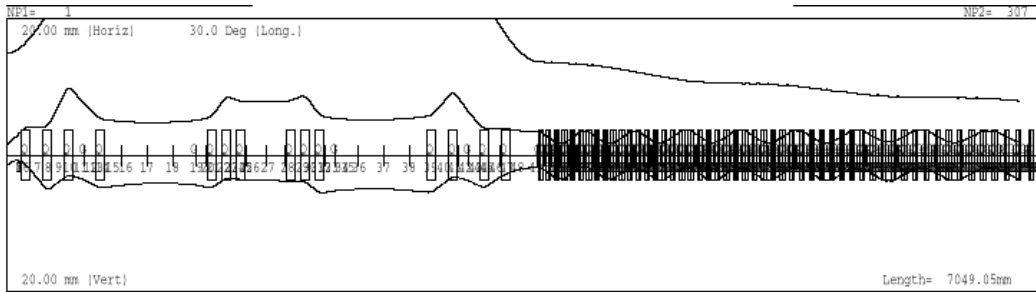


Fig. A.1. Trace3D output of entire MEBT optics modification.

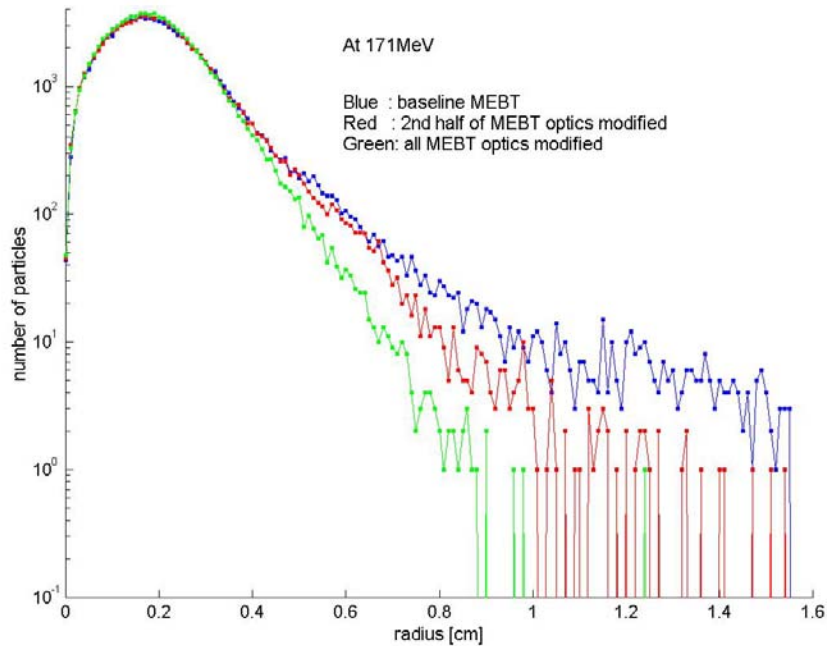
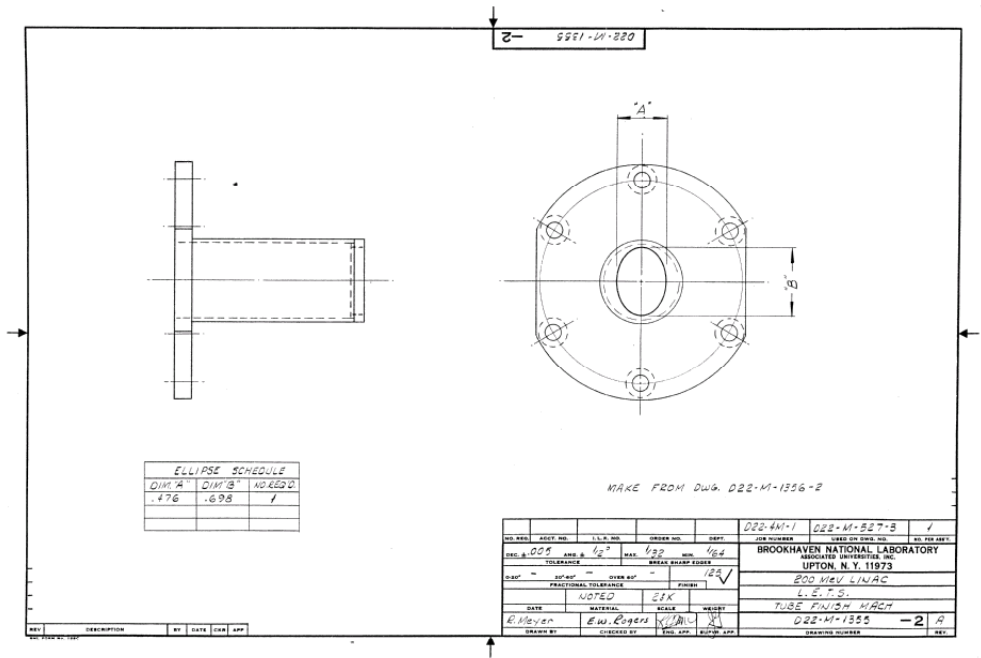


Fig. A.2. Beam profile plots at 171MeV for three different MEBT optics without any collimation. Blue is for the baseline optics, Red for the MEBT with 2<sup>nd</sup> half of optics modified, and green for the MEBT with entire MEBT optics modified. Significant reduction of halo is observed.

## Appendix 2: Beam Scraper at BNL Drift Tube Linac



**Fig. A.3. Schematic drawing of beam scraper for the Drift-Tube-Linac of the 200 MeV Linac at Brookhaven National Laboratory.**

The Brookhaven National Laboratory linac delivers 200 MeV proton or H<sup>+</sup> beams. The first tube of the Drift Tube Linac is fit with an elliptical scraper made of tungsten with only contact cooling with the Cu tube as shown in Fig. A.1. The beam energy at the scraper is 750 keV. In simulation, about 5% of the 100 μA beam is collected by the scraper. The elliptical scraper is rotated by 90 degrees when the beam is switched from proton to H<sup>+</sup> beam.

### **Appendix 3: Beam Scraper at ISIS Drift Tube Linac**

The ISIS linac at the Rutherford-Appleton Laboratory delivers 70 MeV H<sup>+</sup> beams. The first six tubes of the DTL tank 2 are fit with fixed scrapers made of reactor-grade high-density graphite. The scrapers are split longitudinally and sprung into place with only contact cooling to the Cu tube. The inner diameters of the scrapers are progressively reduced along the beam direction.